doi:10.1017/S1431927622001994
Microsc. Microanal. 28 (Suppl 1), 2022

Large Volume 3D Electron Backscatter Diffraction Characterization of Lath Martensite in 13%Cr-4%Ni Stainless Steel by Xe Plasma FIB

Mehdi Mosayebi[1], Hui Yuan[2], Betty Huang[1], Daniel Paquet[3], Pierre-Antony Deschênes[3,4] and Nabil Bassim[1,2*]

[1.] McMaster University, Materials Science and Engineering Department, Hamilton, ON, Canada.
[2.] McMaster University, Canadian Centre for Electron Microscopy, Hamilton, ON, Canada.
[3.] Hydro-Québec, Institut de recherche d'Hydro-Québec, Varennes, QC, Canada.
[4.] Department of Mechanical Engineering, École de technologie supérieure, Montreal, QC, Canada.
* Corresponding author: bassimn@mcmaster.ca

Lath martensite in steel is well known to show a hierarchical microstructure consisting of packets, blocks, sub-blocks, and laths. The prior austenite grain (PAD) is divided into packets and each packet is further subdivided into blocks. Since this complex morphology affects the toughness and strength of steels, clarifying the characteristics of morphology and crystallography of martensite is of great importance [1].

3D characterization techniques have demonstrated great potential to provide important insights into the 3D morphology of complicated microstructures. In cases where high spatial resolution information is required in 3D, serial sectioning techniques have been successfully applied to collect stacks of 2D images which can be aligned in sequence to build up a 3D image of the specimen. As such, serial sectioning with femtosecond laser (Tri-Beam system) offers the ability to gather larger volumes. However, a trade-off is made by sacrificing on the resolution, which is limited to a slice thickness of ~1μm [2]. Using dual-beam FIB-SEM instruments, is a suitable way to achieve high spatial resolution can be provided (~10s of nms [2]). With a conventional Ga^+ FIB, the milling time limits the volume that can be captured in a reasonable amount of time, especially if EBSD data is being collected. Xe^+ plasma FIB (PFIB) allows for faster milling times and larger volumes than conventional Ga^+ FIB and better resolution than Tri-Beam [2]. It is apparent that PFIB can offer an excellent trade-off between collecting data from a large enough volume to be representative of the behavior of the bulk material while maintaining sufficient spatial resolution to observe all relevant features of a complex microstructure. This makes PFIB an excellent choice for investigating the lath martensite structures in steels, especially for crystallographic features of the order of the austenite grain size or larger (~100 μm).

This study aims to deploy large volume PFIB-EBSD to investigate the morphology and crystallography of microstructural features in a quenched 13%Cr–4%Ni stainless-steel (UNS S41500) with an average PAG size of ~80μm. To this end, a volume of roughly 120 × 120 × 60 μm^3 was lifted out for serial sectioning using a dual-beam FEI Helios G4 Xe^+ PFIB. The volume was lifted out using a micromanipulator within the microscope chamber and then attached to a Si substrate using Pt. The Si substrate was then attached to a specifically designed pre-tilted holder for 3D-EBSD experiments (Fig.1). The sectioning and EBSD scans were controlled by the FEI Auto-slice-and-view software. The slice thickness was set to 250 nm and EBSD were collected every other slice for a final z-resolution of 500 nm. A current of 0.2 μA was used for slicing the block, giving a total slice time of ~25s. A 5° rocking mill was also used in order to prevent curtaining effects. EBSD was collected on each slice at 20 keV with a current of 13 nA using an Oxford Symmetry detector and the Aztec control software.

Each EBSD map covered the entire sample face with indexing at 500 nm step size in order to match the final z-resolution of 500 nm and so provide approximately cubic voxels for the 3D reconstructions. The final dataset consisted of 132 individual slices and took ~ 12 hours to collect. Reconstruction steps including importing the raw data, thresholding, alignment, clean-up and segmentation were all carried out in DREAM.3D software [3]. Following reconstruction, the final 3D dataset file was visualised using ParaView [4].

Fig. 2a and b, display two views of the resulting 3D reconstruction of the martensite structure produced with Dream3D software. To identify the PAGs, 2D EBSD data from different depth of the 3D microstructure were used (Fig.2c-f). The PAG reconstruction was carried out using a MATLAB code with the help of MTEX toolbox, originally developed by Nyyssönen [5]. This software utilizes the Kurdjumov–Sachs (K-S) orientation relationship to reconstruct PAGs from the IPF maps of the martensitic microstructure. As can be seen in Fig.2g-k, the 3D dataset contains 5 different PAGs (PAG1-PAG5) that are partially located in the collected dataset. In order to further investigate the crystallography and morphology of the microstructural features in 3D, only PAG1 and PAG5 were subjected to more detailed analysis in Fig.3 and 4. From the EBSD maps showing the IPF and 2D reconstruction of packets for slices 10, 65 and 105 in Fig.3a-f, it can be observed that both PAG1 and PAG5 contain four types of packets (CP1-CP4) which is coherent with the K-S theory. These blocks and their variant pairs are indicated on the corresponding 3D orientation maps of PAG1 and PAG5 in Fig.3d-i. To clarify the morphology of the packets and blocks in both PAG1 and PAG5, 3D reconstruction of some of the larger blocks from all CP1-CP4 packets are presented in Fig. 4a-d. In 2D observations, the morphology of packets is estimated as equiaxed and polyhedral. From 3D observation, however, the packets are plate–like and anisotropic. This observation was also made by Morito et al. [6]. An interesting observation here, is that all these plate-like packets and their blocks in both PAG1 and PAG5 can be classified into 3 different types based on their overall orientation in the sample reference frame, including vertically oriented blocks, horizontally oriented blocks, and ~45°-inclined blocks. It is also obvious that blocks of each type hold crystallographic orientations close to each other in both grains. This study helps with understanding the crystallography, morphology, and their correlation, in a complex martensite structure for sizes of the order of PAG in 3D.

https://doi.org/10.1017/S1431927622001994 Published online by Cambridge University Press

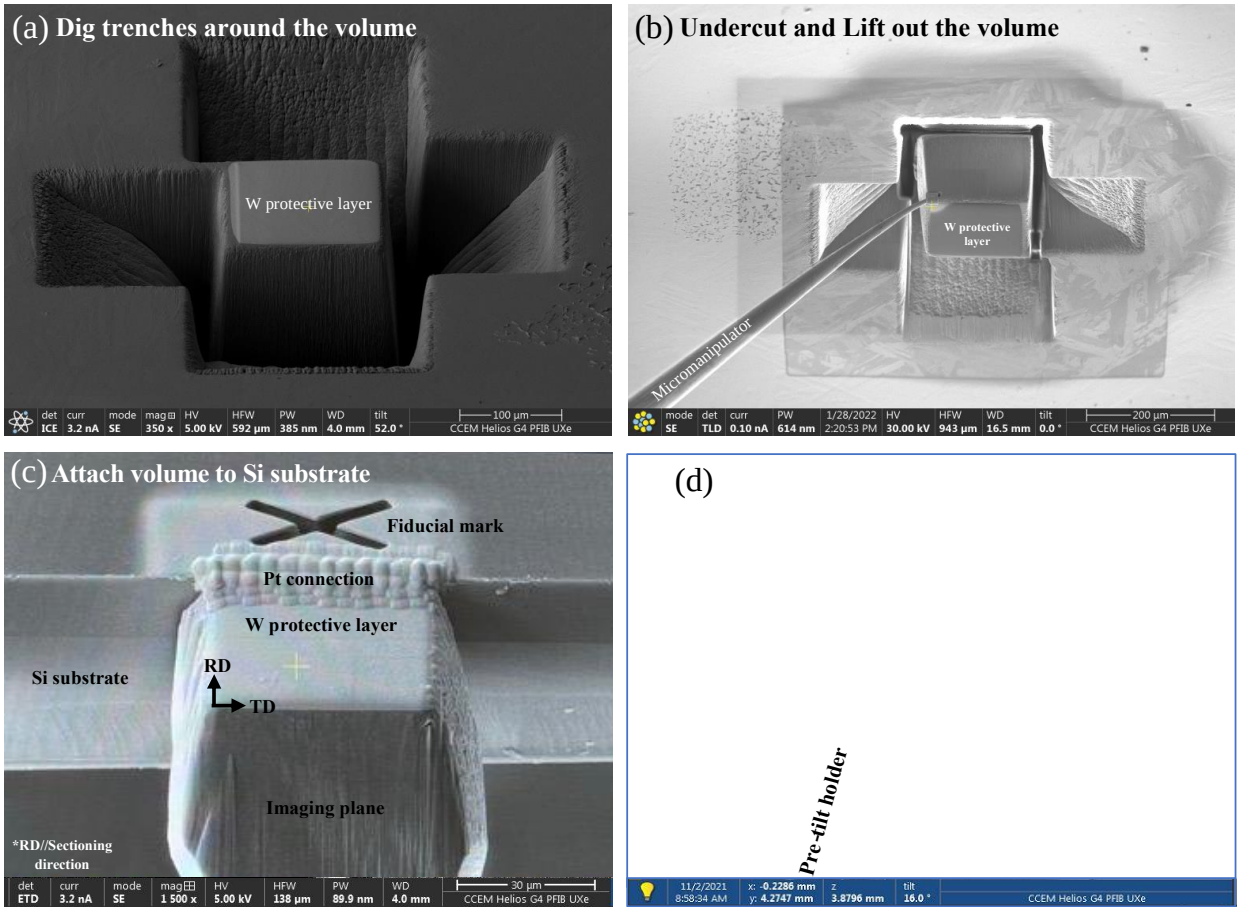

Figure 1. (a-c) Procedure for lifting out the volume for serial sectioning experiment. (d) The configuration of electron column, ion column, EBSD detector and the pre-tilt holder inside the PFIB chamber.

https://doi.org/10.1017/S1431927622001994 Published online by Cambridge University Press

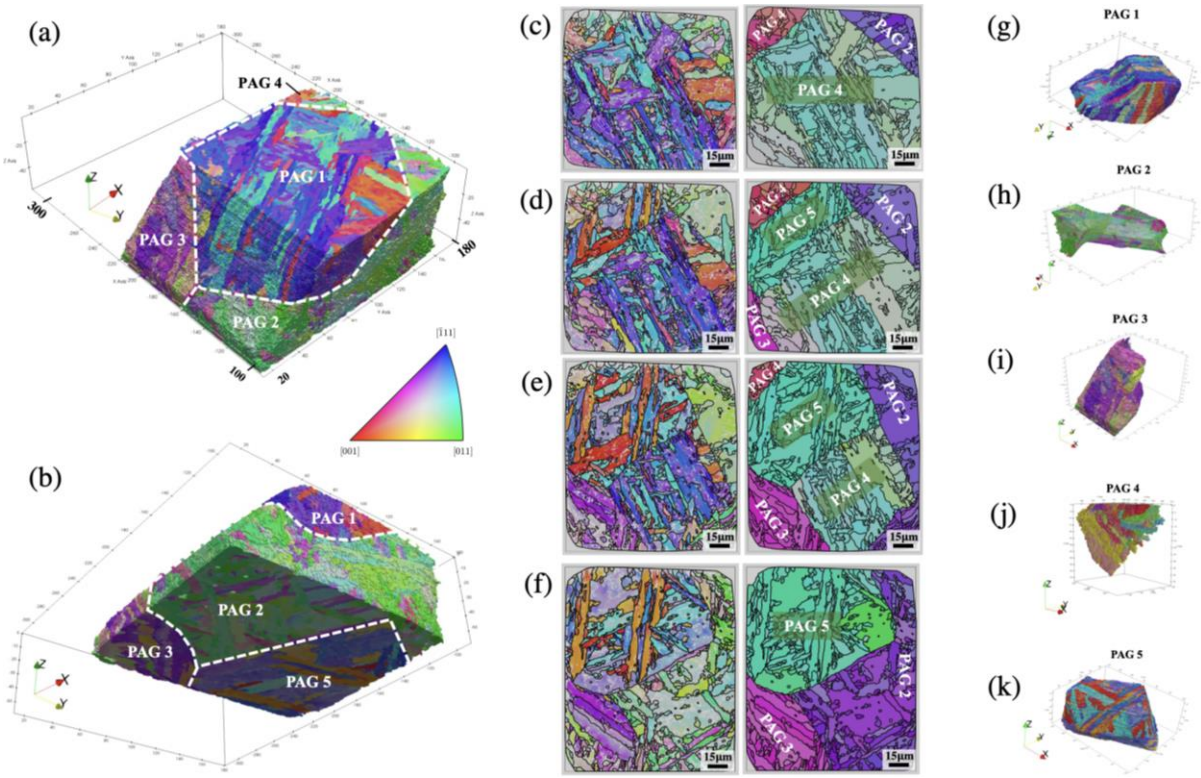

Figure 2. (a and b) 3D reconstruction of the martensite structure produced with Dream3D software. PAG1-PAG5 are defined with white dashed lines. (c-f) 2D-EBSD maps extracted from MTEX toolbox showing the IPF and reconstruction of PAGs for slices 10, 35, 65 and 105 (out of 132 EBSD scans), respectively. (g-k) 3D reconstruction of PAG1-PAG5. (All 2D and 3D orientation maps are color coded with respect to Z//slicing direction)

https://doi.org/10.1017/S1431927622001994 Published online by Cambridge University Press

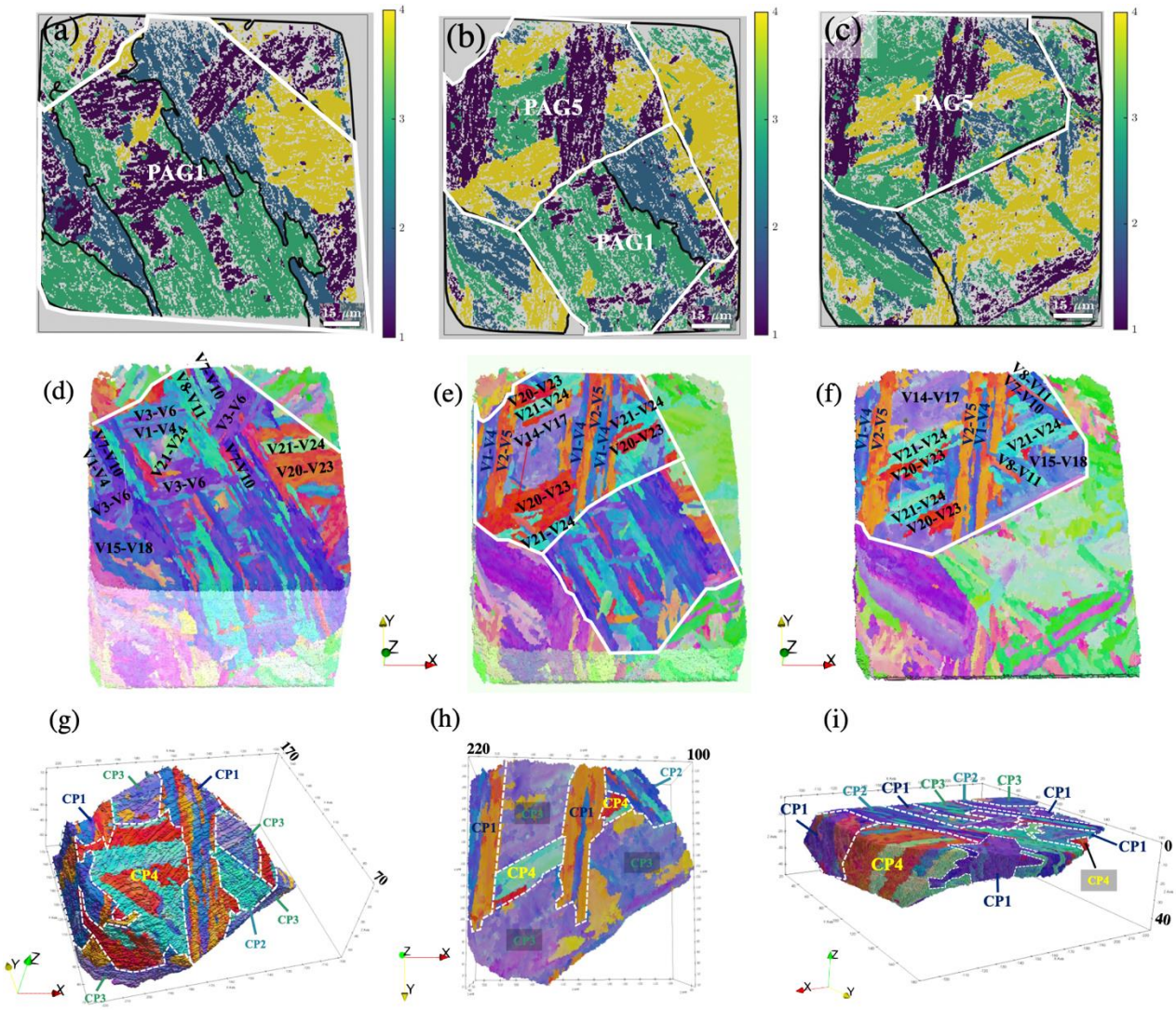

Figure 3. (a-c) 2D-EBSD maps extracted from MTEX toolbox showing the reconstruction of the packets for slices 10, 65 and 105, respectively. (d-f) 2D sections at slices 10, 65 and 105 of the 3D datasets in Fig. 2a and b. Martensitic variants for some of the packets in PAG1 and PAG5 are indicated on the orientation maps in Fig.3d-f. (g-i) 3D reconstruction of PAG5 (g and h) and PAG1 (i) with their packets marked as CP1-CP4. (All 2D and 3D orientation maps are color coded with respect to Z//slicing direction)

https://doi.org/10.1017/S1431927622001994 Published online by Cambridge University Press

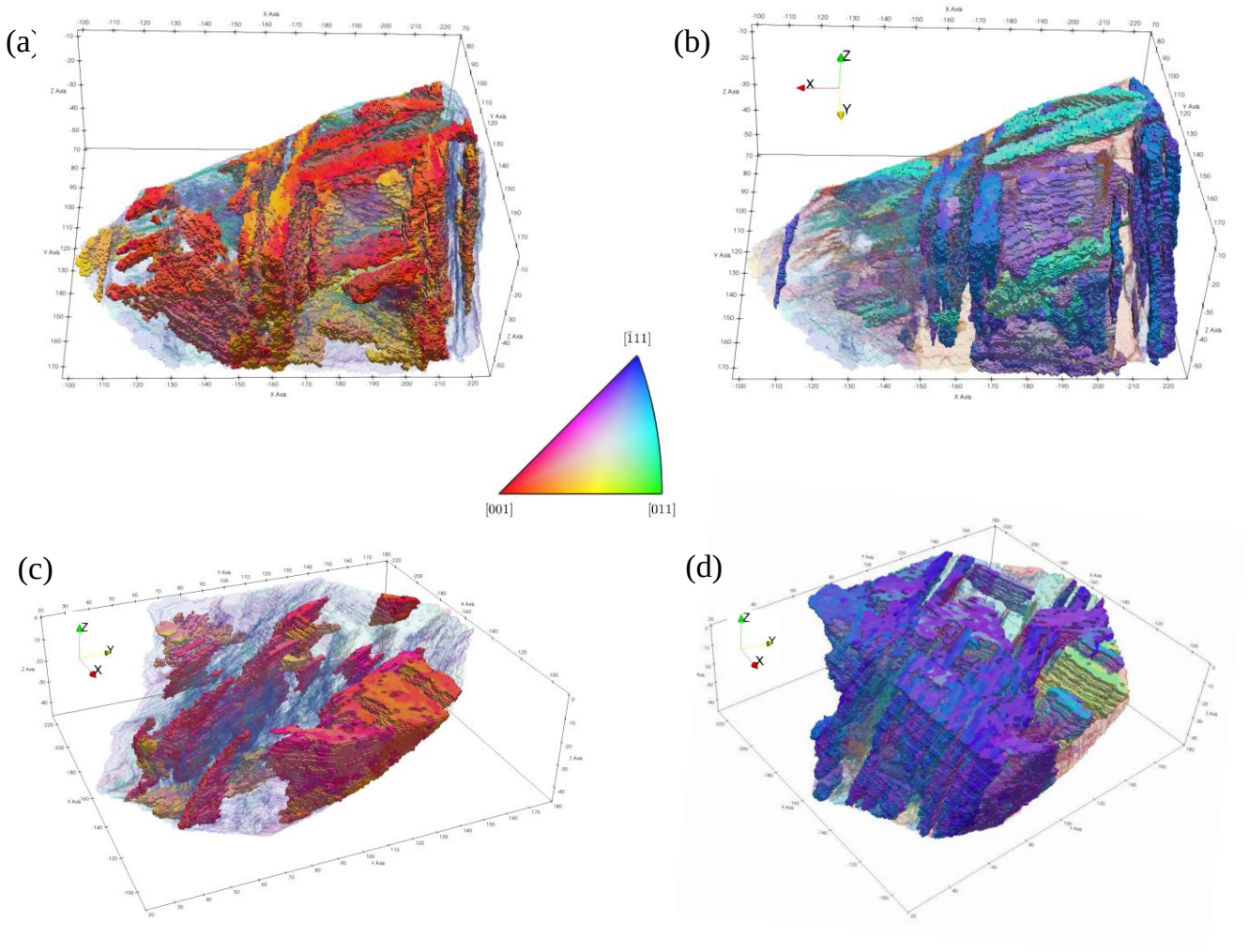

Figure 4. 3D reconstruction of some of the larger blocks from all CP1-CP4 packets for (a and b) PAG5 and (c and d) PAG1.

References:

[1] H Kitahara et al., Acta materialia **54**(5) (2006), p. 1279. https://doi.org/10.1016/j.actamat.2005.11.001
[2] R DeMott et al., Ultramicroscopy **230** (2021), p. 113394. https://doi.org/10.1016/j.ultramic.2021.113394
[3] MA Groeber and MA Jackson, Integrating materials and manufacturing innovation **3**(1) (2014), p. 56. https://doi.org/10.1186/2193-9772-3-5
[4] J Ahrens, B Geveci and C Law, The visualization handbook **717**(8) (2005).
[5] T Nyyssönen et al. Metallurgical and Materials Transactions A **47**(6) (2016), p. 2587. https://doi.org/10.1007/s11661-016-3462-2
[6] S Morito, Y Adachi and T Ohba, Materials transactions **50**(8) (2009), p. 1919. https://doi.org/10.2320/matertrans.MRA2008409

https://doi.org/10.1017/S1431927622001994 Published online by Cambridge University Press